Synthesis and Characterization of Bismuth Ferrite and Lead Zirconium Titanate (BFO-PZT) Laminate Composite

A thesis submitted in partial fulfillment of the requirements for the award of the degree of

Masters of Technology

(Materials and Metallurgy Engineering)

Submitted by

ANOOP PRATAP SINGH

Roll No. 601102002

Under the guidance of

Dr. PUNEET SHARMA

(Assistant Professor)

School of Physics and Materials Science

Thapar University, Patiala-147004,

Punjab (India)

Dedicated to GOD
and My Parents

Aum Bhoor Bhuvah Svah
Tat Savitur Varenyam
Bhargo Devasya Dheemahi
Dhiyo Yo Nah Pracho Dhayãt

Declaration

I hereby declare that the report entitled "**Synthesis and Characterization of Bismuth Ferrite and Lead Zirconium Titanate (BFO-PZT) Laminate Composite"** is an authentic record of my the award of M. Tech. (Materials Science and Metallurgical Engineering) under the supervision of ***Dr. Puneet Sharma,*** School of Physics and Materials Science, Thapar University, Patiala duration January to June 2013.

The matter presented in this M. Tech thesis has been not submitted in directly/ indirectly to another University or Institute for the award of any degree.

Dated: 3/07/13

Anoop Pratap Singh

M. Tech (MME)

Roll. No. 601102002

Above statement and declaration made by candidate is correct to my knowledge and belief.

Dr. Puneet Sharma
Assistant Professor
School of Physics and Materials Science
Thapar University, Patiala (147004)

Countersigned by

Dr. Kulvir Singh
Hear and Associate Professor
School of Physics and Materials Science
Thapar University, Patiala (147004)

Dr. S. K. Mohapatra
Dean Academic Affairs
Thapar University, Patiala (147004)

Acknowledgement

The deep sense of gratitude, I thank all those who have contributed the conception origin and nurturing of this project.

I would like to express my sincere thanks to my M. Tech. Supervisor, ***Dr. Puneet Sharma*** Assistant Professor, School of Physics and Materials Science, Thapar University, Patiala for providing me valuable guidance during the entire project and for providing me his timely support, help and encouragement. His guidance & suggestions were very helpful to shape my research skill. I am sure that the knowledge gained through my association with my supervisor shall go a long way in helping me to achieve goals in my life.

I would like to express my sincere regards to ***Dr. Kulvir Singh,*** Associate Professor and Head, ***Dr B. N. Chudasama,*** Assistant Professor, ***Dr. N. K. Verma***, Senior Professor, School of Physics and Materials Science for providing me facilities without which this work would not be possible. I am also thankful for giving valuable time in support of my knowledge ***Dr. Bonamali Pal***, Associate Professor, ***Dr. Vijay Laxmi***, Assistant Professor, ***Dr. Partho Mohanti***, Assistant Professor and ***Dr. Kalamdeep Paul***, Assistant Professor, School of Chemistry and Biochemistry, Thapar University Patiala.

I would like to put my heartiest gratitude to my parents for their constant co-operation, inspiration, patience, blessing and moral support. I am very greatful thank to the Ph. D. scholars ***Mintu Tyagi*** who give me support in experimental research, theoretical studies and in laboratory works. I am also thanksful for encoragous supports to others Ph.D. Scholars ***Ranvir Panwar, Kapil Sood, Samiksha Verma, Chandni Khurana, Samita Thakur, Meenakshi Batra, and Paramjyot Jha.*** Theie help and cooperation during my study will always be remembered.

In last but not the least I would like to thank all my friends who have helped me directly or indirectly to do my project work.

APSingh

Anoop Pratap Singh

Roll No. 601102002

ABSTRACT

In this study, pure $BiFeO_3$ (BFO) and $Pb(Zr_{0.52}Ti_{0.48})O_3/BiFeO_3$ laminate composite was prepared by sol-gel method. X-ray diffraction studies confirm the formation of single phase polycrystalline BFO and PZT with distorted rhombohedra perovskite structure and tetragonal structure respectively. The effect of PZT layer on the ferroelectric and dielectric properties of BFO has been studied. The composite structure exhibits the good ferroelectric and dielectric properties at room temperature. The electric properties of composite are improved by stacking of PZT layer on BFO. The relative dielectric constant of pure BFO and composite BFO-PZT were found to be 240 and 270 respectively. The saturation polarization (P_s) was found to be 20 $\mu C/cm^2$ for pure BFO and 40 $\mu C/cm^2$ for BFO-PZT composite structure**.**

List of Contents

List of Figures

Chapter 1

INTRODUCTION

1.1 Multiferroic Materials

Multiferroics are multifunctional materials that simultaneously possess two or more ferroic orders such as ferroelectric and ferromagnetic. In recent years this term is used for the materials in which magnetism and ferroelectricity coexist. The coexistence of these properties is reported in literature for single phase as well as multiphase composite materials [1-6]. ***In 1894, P. Cuire*** predicted [7] that crystals could be simultaneously ferromagnetic and ferroelectric. The magnetization in the crystal can be induced by the application of electric field and vice-versa. This effect is known as magnetoelectric effect. Multiferroic composites combining a ferroelectric and ferrimagnetic phase generated interest because of their applications promised for numerous types of novel multifunctional devices, such as in information storage, sensors and spintronics etc [7]. $BiFeO_3$ (BFO) is a well known multiferroic material that exhibits a distorted pervoskite structure with rhombohedral symmetry. Being a room temperature multiferroic (T_C = 1123 K and T_N = 643 K), it has been widely studied [2, 6]. and known to exhibit excellent ferroelectric properties with large remnant polarization. However, considerable drawback that limit their multifunctional applications is the weak magnetic behaviour such as low saturated magnetization and remnant magnetization because of its G-type antiferromagnetic structure with nearest neighbour spins canting [8,9].

In recent years, the BFO has been much interest due to its ferro-electricity and anti-ferromagnetism at room temperature. The pure BFO has weak ferroelectric and magnetism at room temperature. It has high leakage current density. Several efforts have been done to reduce its leakage current density (J) and to improve its ferroelectric and ferromagnetic properties. In this fashion many dopant, co-dopant and composites have been develop to improve the ferroelectric, ferromagnetic and simultaneouly to improve the insulating behaviour of BFO[3-6]

1.2 Types of Multiferroics

The microscopic origin of magnetism is basically the same in all magnets; it is the presence of localized electrons, mostly in the partially filled *d* or *f* shells of transition metal or rare earth ions, which have corresponding localized spin, or magnetic moment. Exchange interactions between localized moments lead to magnetic order. However the situation is different in case of ferroelectrics. There are several different microscopic origins of ferroelectricity and accordingly one can have different types of multiferroics. Generally the multiferroics are categorized in two groups:

(i) Type I multiferroics
(ii) Type II multiferroics

1.2.1 Type I Multiferroics

This group of multiferroics contains those perovskites in which ferroelectricity and ferromagnetism have different sources (cations at A-site and B-site respectively). These materials show weak magnetoelectric coupling. In these materials, ferroelectricity typically appears at higher temperatures than magnetism and they exhibit large spontaneous polarization. Examples are $BiFeO_3$ (T_c^{FE} ~ 1110 K, T_N ~ 643 K, P ~ 90 μC/cm^2), $YMnO_3$ (T_c^{FE} ~ 914 K, T_N ~ 76 K, P ~ 6 μC/cm^2). However, major challenge in these materials is to enhance the values of magnetoelectric coupling coefficient. Type I multiferroics are further classified in many subclasses on the basis of origin of ferroelectricity.

(*i*) Ferroelectricity due to shifting of B-cation

There are a number of perovskites materials reported that show ferroelectricity due to non-centrosymmetry of B- site cation [6].

(ii) Ferroelectricity due to lone pairs

Fig. 1.1 shows the ferroelectricity due to lone pair at A-site cation. Most of Bismuth (Bi) and Lead (Pb) based perovskites show ferroelectricity due to lone pair, for example $BiFeO_3$, $BiMnO_3$, and $PbVO_3$. In these materials Bi^{3+} and Pb^{2+} have two outer 6*s*

electrons that do not participate in chemical bonds. These electrons are called "lone pairs" or some times dangling bonds. Microscopically, one can explain the origin of ferroelectricity in these compounds by the ordering of these lone pairs (with certain admixture of *p*-orbitals) in the direction of electric field.

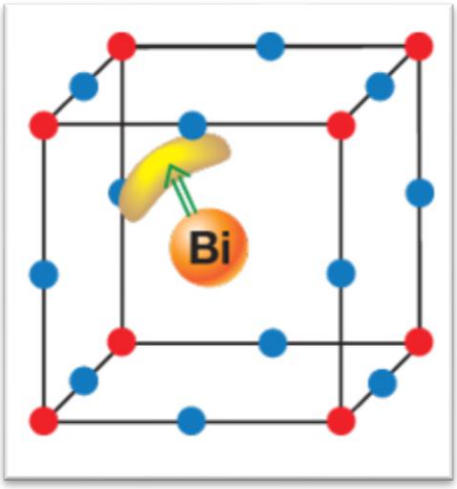

Fig. 1.1: In materials like $BiFeO_3$ and $PbVO_3$, the ordering of lone pairs (yellow "lobes") of Bi^{3+} and Pb^{2+}ions (orange), contributes to the polarization (green arrow).

(iii) Ferroelectricity due to charge ordering

This is another group of ferroelectrics, in which the electric polarization is induced due to the non-centrosymmetry of charges. The non-centrosymmetry of charges is normally observed in transition metal compounds (especially transition metal ions with different metal states) e.g. $Pr_{0.5}Ca_{0.5}MnO_3$ or in Nickelates $RNiO_3$ [6,7].

(iv) Geometrical ferroelectricity

In this category of multiferroics, some gerometric disorder in the lattice causes ferroelectricity. For example in case of $YMnO_3$, ferroelectricity has nothing to do with individual cations, but is caused by the tilting of practically rigid MnO_5 block with respect to Y-ions.

1.2.2 Type II Multiferroics (Magnetic Multiferroics)

The materials in which the ferroelectricity is originated from magnetism and implies strong magnetoelectric coupling. However the polarization in these materials is usually much smaller (10^{-2} μC/cm^2). These multiferroics are recently discovered. $TbMnO_3$ and $TbMn_2O_5$ are typical examples of these materials [9]. The polarization changes sign with magnetic field. Since the discovery of these materials, a number of other type-II multiferroics with strong magnetoelectric coupling have been discovered and studied. On the basis of mechanism of multiferroic behavior, one can divide type-II multiferroics in two categories

(i) Spiral Type-II Multiferroics

In this type of multiferroics, the ferroelectricity appears in conjunction with a spiraling magnetic phase, mostly cycloid type. $TbMnO_3$, $Ni_3V_2O_6$ and $MnWO_4$ are typical examples of this type of multiferroics. Fig.1.2 shows the G-type spin cycloid antiferromagnetic structure.

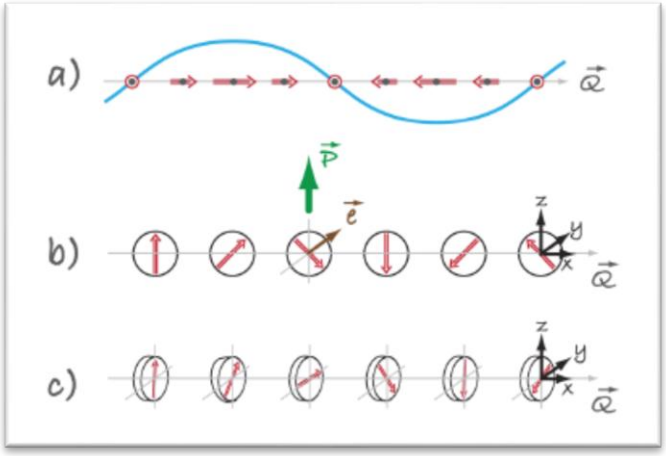

Fig. 1.2: Different types of spin cycloid structures relevant for type-II multiferroics.

1.3 Bismuth ferrite ($BiFeO_3$)

The famous multiferroics material is $BiFeO_3$, it is generally denoted by BFO shortly in material science and engineering. The BFO is an organic compound which holds constituents as bismuth, iron and oxygen respectively. It is a lead free material. It is not

harmful for the environment and human beings. At room temperature it possesses multiferroic properties and also shows piezoelectric properties. The BFO has transition temperature (1103℃) and single BFO crystal has a high electric polarization than other ferroelectrics.

1.3.1 Phase diagram of BFO

Fig.1.3 shows the compositional variation phase diagram of BFO. The BFO is prepared from the equal ratio of both Bi_2O_3 and Fe_2O_3 at high temperature (about 800℃) via the following equation-

$$Fe_2O_3 + Bi_2O_3 \longrightarrow 2\ BiFeO_3$$

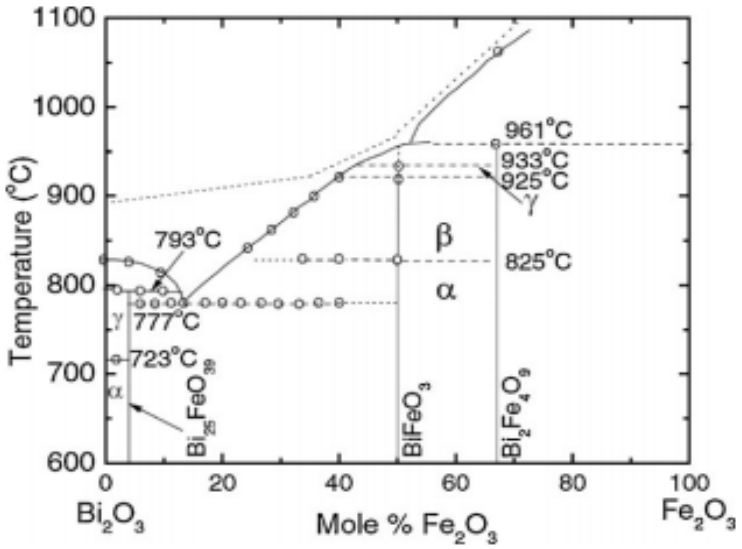

Fig. 1.3: Compositional phase diagram of BFO [10]

The bismuth ferrite is very prone to illustrate parasitic phase that nucleate at the grain boundaries and impurities [11]. Below the melting temperature (270℃) BFO has metastable state in air and optically impurities spots appears [12-14]. The impurities and oxygen vacancies artificially improves the remnant magnetization [15,16]. At room temperature if 200kV/cm electric field applied then BFO decompose yielding magnetite Fe_3O_4 as by product [17].

$$6BiFeO_3 \longrightarrow 2Fe_3O_4 + 3Bi_2O_3 + O$$

The Bi_2O_3 phase is not detected because probably it is glass forming compound or vaporization during thermal decomposition (M. P. ~800℃ [10]). This decomposition gives the new explanation to remnant magnetization in BFO.

1.3.2 The Structure of BFO

Fig. 1.4 shows the the crystal structure of BFO.The spontaneous polarization direction (*Ps*) and antiferromagnetic ordering (gray) are mentioned in this fig. At room temperature the phase of BFO is a rhombohedral (point group R3c) [18]. The perovskite type unit cell has a lattice a_{rh} =3.965 A^0 and rhombohedral angle α_{rh}= 89.3°-89.4° room temperature[19,20], with ferroelectric polarization along $[111]_{pseudocubic}$ [20]. The unit cell atcan also be described in a hexagonal frame of reference with the hexagonal c-axis parallel to diagonal of the perovskite cubice as$[001]_{hexagonal}$ parallel $[111]_{pseudocubic}$. The hexagonal lattice parameter are a_{hexa}=5.58 A^0 and c_{hexa}= 13.90 A^0[19-21]. The very important structure parameter is the rotation of oxygen octahedral. This angle would be 0 degree for cubic perovskite with perfect match ionic size. Fe-O-Fe angle is important because it control to magnetic exchange and orbital overlap between Fe and O.

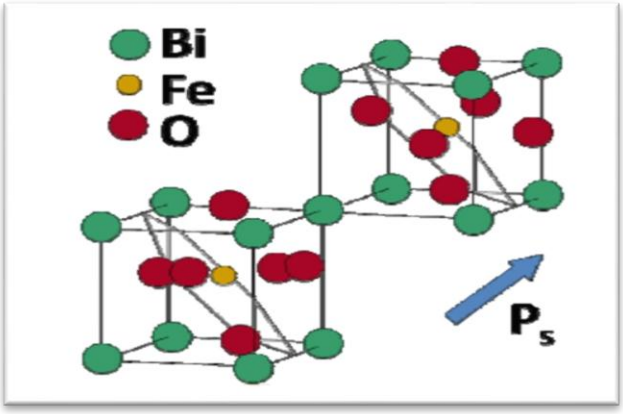

Fig.1.4: Schematic of BFO crystal structure[22].

1.3.3 Properties of BFO

1. The dielectric constant (ε_r) and loss $tan\delta$ is the function of the temperature. If the temperature increases the dielectric constant and dielectric loss also increases respectively.

2. The spontaneous polarization is lower than ferroelectric materials.
3. Pure BFO has weak properties in bulk form. If less amout of dopant is used then leakage current density reduces and if solid state solution of BFO made with other perovskite then the leakage current density also reduces [23]. This gives a multiferroic hetero-structure. A single crystal of BFO at room temperature does not provide any P-E loop information. If defects are present in the BFO then it shows conducting characteristicsts make difficulty in measuring the hysteresis loop.
4. Antiferromagnetic ordering: BFO shows *G-type* antiferromagnetic ordering at room temperature.

1.4 Piezoelectric Ceramic Materials

The term piezoelectric ceramic was investigated in 1941. The piezoelectric ceramic materials have important place in material science and engineering industries[24].There are three basic steps in discovery and understanding of piezoelectric ceramic materials-

1. Dielectric constant
2. To realize the cause of the high dielectric constant was ferroelectricity.
3. The significant discovery was of the poling process.

The piezoelectric ceramic showed the connection between piezoelectricity and crystal symmetry. There were a few isolated observations of real and apparent piezoelectric effect in nonsingle crystal media such as polarized waxes, wood and ebony. But these effects were unfit and weak to technical applications. The first ferroelctricity was discovered by on a single crystal, Rochelle salt [25].

The refractory ceramic oxide prepared **in 1941** by ***Thurnauer and Deaderick***[26,27] at American Lava Co. company and its name was Barium oxide-titanium oxide composition. This showed high dielectric constant 1100 than the Rutile. The best conventional piezoelectric materials are $BaTiO_3$ and $Pb(Ti,Zr)O_3$, both of them shows the weak in electromechanic poling factor and mechanical quality factor.

To object of this investigation is to provide a novel piezoelectric ceramic material, having large values of both electromechanical coupling factor and mechanical quality factor. These piezoelectric ceramic materials suited for use in various field as like manufacture or ceramic filters and transducer of mechanical filters. The member of this family is lead zirconium titanate.

1.4.1 Lead Zirconium Titanate (PZT)

Among bulk materials, the PZT is known to be one of the strongest piezoelectric, with extremely high piezoelectric coefficients and electromechanical coupling factor. Reproducing these properties in bulk form, however, require precise control of composition and texture. The aim is to develop maximize crystallinity and minimize resistivity through precursor modification and thermal treatments**.**

1.4.1.1 Ferroelectricity and Piezoelectricity in Crystals

Ferroelectricity and piezoelectricity in crystals can be explained on the basis of symmetry operations. It is found that symmetry operations can be combined in 32 different ways, resulting in 32 different crystal classes. Out of these 32, only eleven crystal classes have center of symmetry and 21 have non-centro symmetry. Further out of the remaining 21 non centro-symmetric, only 20 show piezoelectricity. The remaining one non-centro symmetric class left does not show any piezoelectric effect because of the combined effect of symmetry. Piezoelectric effect is the phenomenon of creation of electric polarization on the application of external stress and vice-versa. Out of these 20 piezoelectric crystals only 10 posses spontaneous polarization. They are also known as pyroelectric crystals. Pyroelectric effect is the appearance of an electric charge at the surface of the material with change in ambient temperature. Further a current is generated when they are heated or cooled. These currents are generated due to these electrical charges and are called pyroelectric current. Ferroelectricity appear only in few crystal classes out of 10 pyroelectric classes. Ferroelectricity is defined as electrically switchable polarization in crystals. These crystals show large dielectric constant and high coupling factor. Polycrystalline ceramics of these materials show ferroelectric effect only after poling or aligning the dipoles.

1.4.1.2 Pervoskite Structure of PZT

A pervoskite type of crystal structure shown in fig. 1.5 by compounds has ABO_3 chemical formula**.** There is a cubic arrangement with A atomic surrounded by 12, O atoms and B atom surrounded by 6 O atoms. Example of the Pervoskite structure includes PZT (Lead Zirconium Titanium oxide), BFO (Bismuth ferrite) and LF (Lanthanum ferrite).

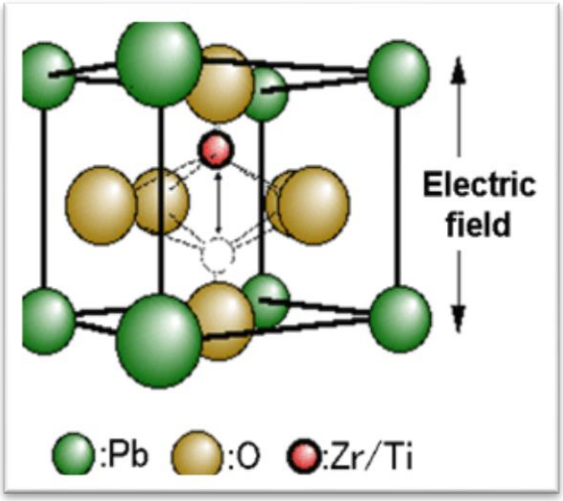

Fig.1.5: Atomic arrangement of the pervoskite structure (ABO_3), where 'A' and 'B' are two cations of different size, and 'O' is an anion that bond to both

1.4.1.3 Phase diagram of {Pb ($Zr_{.52}Ti_{.48}$) O_3}

The phase diagram of the PZT system, shown in fig. 1.6, provides a useful way to classify the behavior of PZT. A continuous solid solution exists between $PbTiO_3$ and $PbZrO_3$ as shown in the figure 1.6. Pure $PbTiO_3$ has the tetragonal perovskite structure and is ferroelectric in nature.

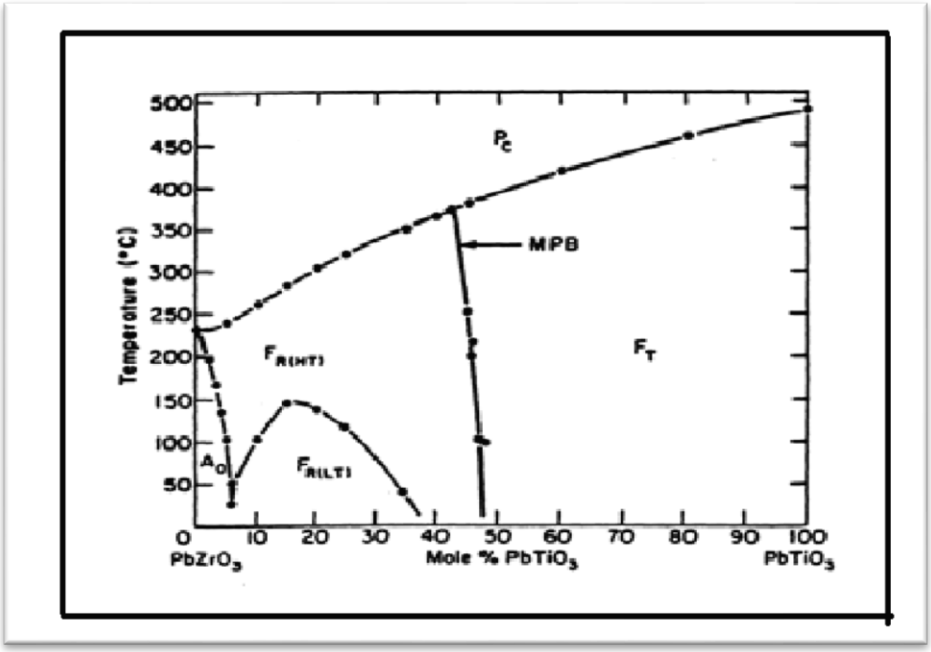

Fig. 1.6: Phase diagram of {Pb ($Zr_{.52}Ti_{.48}$) O_3}. [28]

1.4.1.4 The Characteristics of PZT

1. High output,low drive material
2. High frequency, fast response time
3. Ability to use with low voltage or high voltage drive circuits
4. Good mechanical and acoustic coupling.
5. Wide variety of compositions, shapes and sizes that can be customized to meet the specific and desired applications.

1.4.1.5 Applications of PZT Ceramic Material

The applications of PZT ceramic materials are widely used in memory devices and recording media. The PZT can also use in capacitor, sensors (gas sensor, signal sensor, heat sensor) actuators, and energy harvesting and infrared detectors.

1.4.1.6 Ceramic Material Synthesis Techniques (Powder Synthesis Methods)

There are several methods for the synthesis of ceramic materials.The brief description of most commonly methods are given below

1. Solid State Synthesis method
2. Sol-gel method.
3. High energy ball milling method

1.4.1.6.1 Solid State Reaction method

The Solid State Reaction is also known as dry media reaction or solvent less reaction. The solid state reaction method use for preparation polycrystalline materials. The solid reactant reacts and forms a new substance phase during the complete reaction. The residual wastage removes in the form of a gas after the finishing reaction. These solids normally are not reacting at room temperature. If the temperature is higher (1000 to 1500℃) then reaction occurs in appreciable rate. This reaction affects from the structural properties of the solid reactants, surface area of solid and its reactivity and thermo-dynamical potential [29]. The final products can the either metal oxide, sulphides and nitrides.

1.4.1.6.2 Sol-gel method

The sol-gel method was developed in 1960 during the material synthesis. This method is used for metal oxides fabrication. The sol-gel method is can be defined as- "Formation of an oxide network through poly-condensation reactions of a molecular precursor in a liquid." A sol is the form of suspended colloidal solid particles (1-100nm diameters) in liquid medium. If solid particle has the smaller size than the liquid medium particle, the solid particle disperses in the medium under the other forces besides gravitational force. A gel form is associate with the three dimensional internal stable and expanded network in the liquid medium. When the colloidal particles agglomerated in a gel network, it called colloidal gel. The repeated chain of colloidal gel makes a polymeric substructure, called polymeric gel. The sol particles interact via Vander Waals forces or hydrogen

bonds. The centrifugation is also used for accelerate the phase formation process. The gel process is irreversible and covalent in nature. This gelation process possesses the reversible nature if the other interactions are present in the network formation.

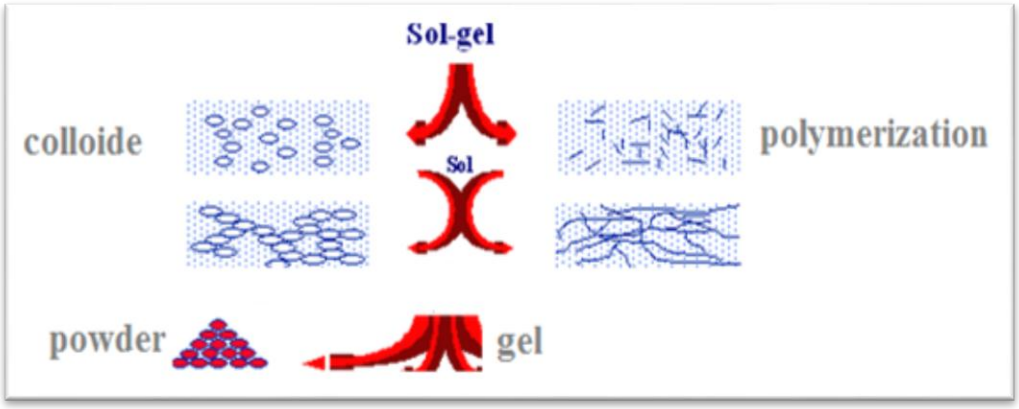

Fig.1.7: sol-gel processing rout [30]

The sol-gel method modified in the two ways-

(1) Colloidal rout

Metal is present in the form of aqua solution and controls both PH value and temperature.

Hydrolysis- $M(H_2O)_n^{Z} \longleftrightarrow \{M(H2O)_{n-1}OH\}^{(Z-1)} + H^{+}$

Condensation and Polymerization-

$M(H_2O)_n^{Z} \longleftrightarrow \{(H2O)_{n-1} M(OH)_2 M(H_2O)_{n-1}\}^{2(Z-1)} + 2H^{+}$

(2) Metal organic rout

Metal oxide in alcoholic solution and water added into it.

- Acid catalyzed hydrolysis

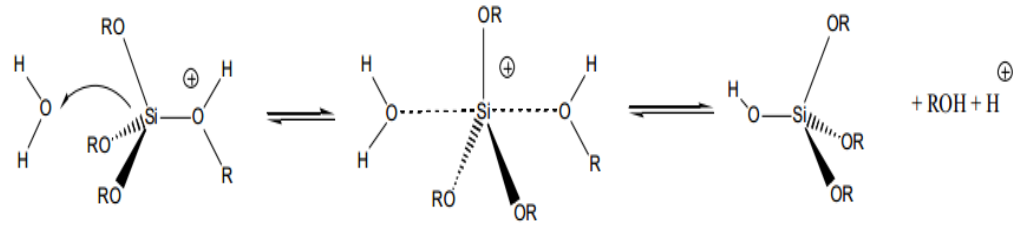

- Base catalyzed hydrolysis

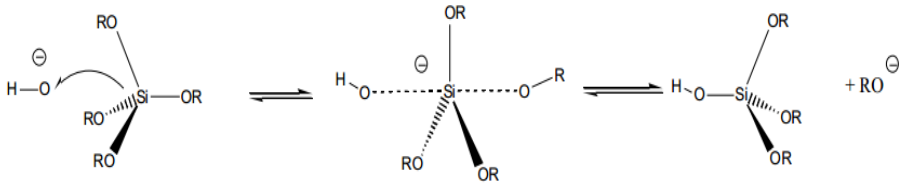

The sol-gel method is popular as provide good control over stoichiometry and reduced sintering temperature. ($PbZr_{1-x}Ti_xO_3$) is a very important material. The largest piezoelectric response is obtained for x = 0.47. The stoichiometry is difficult to control be the ceramic method, where heating at1100˚C for several hours is needed.

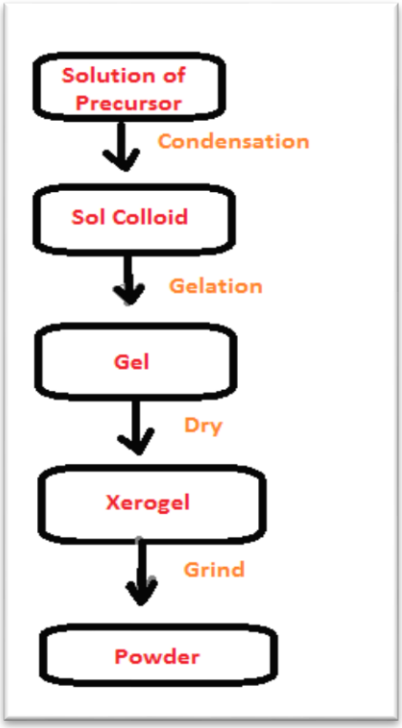

Fig. 1.8: Flow chart of Sol-Gel method

1.4.1.6.3 High Energy ball milling method

The mainly mechanical method is high energy ball milling methods. The principle of ball mills based on the speed of the steels balls which are responsible for the grinding of the particles. Ball milling extensible is used in mechanical alloy processing. The ball milling is the key of equipment of grinding and crushing the material and finally produces the powder. The main parameters of grinding material are density, hardness, size and

composition. The high quality ball milling is potentially expensive and has ability to grind mixture particle in the size limit 5nm. These particles achieve the new surface areas which preferred the reaction rates and decide the nature of the final product. Sometimes the grinding chamber filled with inert gases so that the material did not react with the balls and this medium prevents the oxidation of using material.

1.4.2 Multiferroic bulk ceramic composites

As for piezoelectric composites, the ME composites could have various connectivity schemes, but the common connectivity schemes are 0-3–type particulate composites of piezoelectric and magnetic oxide grains, 2-2–type laminate ceramic composites consisting of piezoelectric and magnetic oxide layers, and 1-3–type fiber composites with fibers of one phase embedded in the matrix of another phase, e.g. $BaTiO_3$, PZT, Pb $(MgNb)O_3$ $–PbTiO_3$ etc., are usually chosen as the piezoelectric ceramic phase, and ferrites usually as the magnetic phase. The leakage problem due to high concentration of the ferrite phase with low resistivity in the particulate composite ceramics can be eliminated in the laminate 2–2 composite ceramics. Laminate composite ceramics are generally fabricated by cofiring ferrite and piezoelectric ceramic layers at high temperature. ME behavior in laminate composite ceramics has been reported for various material couples including PZT or $Pb(Mg,Nb)O_3$–$PbTiO_3$, (PMN-PT) layers laminated with Ni-ferrite (e.g., NFO), or Co ferrite (e.g., CFO) and Bi-ferrite (e,g, BFO). A laminate composite ceramic exhibits higher ME response than its corresponding particulate composite ceramic. Another remarkable difference between the laminate and particulate composite ceramics is that the laminate ceramics exhibit much larger anisotropy than the particulate ones.

The most common 2–2 laminate ME composite is a simple bilayer structure of a ferrite and piezoelectric ceramic layer or sandwich structure, with a ferrite layer (or piezoelectric ceramic layer) sandwiched between two piezoelectric (or ferrite) ceramic layers, which is easily obtained by a sol-gel and conventional solid state reaction method. In this study BFO is choosen as a promising ferroelectric material for high-density FeREMs because of its large remanent polarization. However, BFO has serious problems

as a ferroelectric material, having quite a large leakage current density, especially at room temperature. Therefore, dielectric breakdown occurs easily even at a low field, thereby indicating the difficulty in poling films. Furthermore, the highly electrically conductive nature of BFO makes it difficult to obtain excellent ferroelectric properties. To overcome this problem, various approaches have been proposed, including a substitution technique using Mn, Ti at the B-site, and/or La and Nd at the A-site and the formation of a solid solution with Pb(Zr, Ti)O_3 and $BaTiO_3$ compositions. So in search to improve the ferroelectric properties, dielectric properties and simultaneously to overcome the problem of leakage current density, the BFO/PZT multilayer laminate composites were prepared in the present work and its structural and ferroelctric properties were studied.

Chapter 2

LITERATURE REVIEW

The Bismuth Ferrite (BFO) and lead Zirconium Titanate (PZT) have the great interest due to high remnant magnetization and coercivity in recording and storage media. Various work has been done on both BFO and PZT. In recent years the extensive work has been done to understanding the effect of various dopent and co-dopant in BFO and PZT materials. In present work has been done on PZT (20%) mixed in BFO (80%) matrix. These dopant and co-dopent are enhanced the electric, magnetic properties and are reduced the leakage current densities. In this manner the dielectric constant increases more time than pure BFO and PZT. This material chosen as the multifunctional and single phase material and it reduced the size of storage devices. The work done in few past years on different processing methods and different dopent and co-dopent are given below-

Choudhary et al. in 2006 [31] studied the electrical properties of the BFO-PZT Composite. The BFO-PZT was prepared by Solid State Reaction in single phase ($0.15 \leq x \leq 0.50$). The dielectric loss factor ($\tan\delta$) of BFO was reduced in mixing PZT in BFO matrix. If PZT mixed with the fewest amount then the dielectric constant increased and if again PZT content increased (> 25%) then accordingly dielectric constant reduced. If the activation energy $(0.23 - 0.46\ eV)$was not equal to the lattice energy, then the space charge (distorted structure) and oxygen vacancies gave major role in the conduction of the composition. The dielectric constant also changed by changing the frequencies.

Jo et al. in 2012 [32] fabricated PZT/BFO six times coated thin film. This film had void free and uniform structured grains. This means that some charges occupied the region where the defects or vacancies were present. In this case, the dielectric constant and the dielectric loss was 405 and 0.03% respectively. If the number of multilayers increased then the coercivety 41.3 $\mu C/cm^2$ and remanent polarization increased (15.1MV/cm). The leakage current density at 5V was noted 2.52×10^{-7} A/cm^2.

Wang et al. in 2010 [33] studied the inductions of the strain in one component. This strain produced by themagnetostriction in the ferromagnet or the piezoelectric effect in the ferromagnetic. This strain referred to another component and effectively changed the magnetic field or polarization. He studied how magnetic fields control of electric field (magneto-electric coupling) in the compositional system. The green function, phase field model and first principle method fully explained the ME coupling in Nanostructured material (Vertical hetero-structure, horizontal hetero-structure and particulate nano-composite).

Li et al. in 2005 [34] suggested that a chemical solution deposited film on Pt coated silicon had more remnant polarization ($12\mu C/cm^2$) than the pure formed BFO film. The P-E loop showed the domain wall occlusion in the motion. Frequently in the multilayered film reduced their dielectric loss than PZT film, this was because domain wall restricted the motion. The multilayered film was antiferromagnetic in nature.

Zhang et al. in 2012 [35] investigated that if a BFO/PZT film annealed in the presence of the applied field, then magnetization and electric polarization increased in order of six times more than the zero fields. The saturation magnetization and double remnant polarization was achieved six times more in the presence of the field than in the absence. This magnetic annealed film gave highly performed BFO film.

Nam et al. in 2010 [36] fabricated BFO/PZT six times coated hetero-layered film. This film had void free and uniform grain structure. This was because of the defect part compensated by another layer of coated film. The dielectric constant at 1 kHz was 1360. This dielectric constant increased by increased the order of the coated layers of film. The lower layer of PZT applied compressive stress to upper BFO layer and then BFO layer had distorted rhombohedral structure. This system illustrated the dielectric dispersion nature in the film/film and film/electrode interface by the space charge.

Jo et al. in 2011 [37] synthesizes six layered PZT/BFO thin film. The grain size was smaller than the single PZT films. This grain was uniform and voids free because of their lower layer of BFO provide nucleation sites to PZT layer. The dielectric constant (162)

and dielectric loss (0.017) at applied frequency 1 kHz. The remanent polarization and coercive field of third layered PZT/BFO film were 13.86μC/cm^2 and 37kV/cm.

Xie et al.in 2009 [38] worked on BFO/PZT multilayer capacitor. The PZT buffer layer was formed by MOCVD and sputtering method. The remanent polarization of BFO/PZT (made by MOCVD) was 82.5μC/cm^2 at 8V applied voltage. But in BFO/PZT (made by sputtering, it was 25.2μC/cm^2. The leakage current density (2×10^{-7} A/cm^2) and fatigue polarization up to 10^{10} switching cycles at 4V applied voltage in BFO/PZT_1. The MOCVD coated PZT layer had much induced effect than other PZT coated layers.

Lee et al. in 2012 [39] discovered that the PZT/BFO thin film had changed lattice constant and made a polycrystalline perovskite structure. The lower layer of PZT had controlled the microstructure of the film.The SiO_2 and Ti also incorporated in diffusion.

Hyun in 2011 [40] explored that if multiferroic BFO/PZT (5/95) film was prepared by spin coated method, the structure of the film was polycrystalline perovskite (not $Bi_2Fe_4O_3$). The dielectric properties like dielectric constant and dielectric loss increased with increasing frequencies. The sixth times coated BFO/PZT film showed remanent polarization, dielectric constant and dielectric loss 12μC/cm^2, 0.23% and 1199 respectively.

Wu et al. in 2008 [41] prepared BFO-PZT thin film by electrophoretic deposition method, in which BFO nano particles distributed in the PZT matrix. The BFO structure was distorted by the BFO-PZT core structure. This composition showed Ferro-electricity, ferromagnetism and magneto-electric effect with improved nature. Now days this method is used in magneto-electric and multiferroic based materials.

Stancu et al. in 2011 [42] studied the effect of interface in the different layer on the microscopic properties. The capacitance-voltage, ferroelectric parameters and magnetic hysteresis loop all depended on the number of multilayers. If the number of multilayers was increased, then the degree of disorder increases in the magnetic dipoles. A low applied magnetic field gave the thermal potential to be disordered magnetic dipole and shifted to antiferromagnetic phase.

Jo in 2012 [43] discovered that PZT/BFO had polycrystalline rhombohedra structure. The formed grain had void free and uniform flat surface (40nm in one cycle). If coated layer is increased then Pd diffused from PZT into Pt electrode (down) and Ti diffused fast in the increased annealing process. Due to this diffusion (Pt/Ti and PZT/ Pt) the interface became rough because of the charges accommodated on the interface surface.

Wang et al. in 2009 [44] deposited thin film on BNdT/Ptand PZT/Pt. The metal-ferroelectric-metal structure gave left to right movable capacitance–voltage hysteresis loop because multilayered thin film found ferroelectric polarization. At applied 8V voltage the remanent polarization of BFO/PZT was (23.2μC/cm^2) and PZT/BFO was (45.1μC/cm^2). The leakage current density of Pt/BFO/BNdT/Pt was 3×10^{-5} A/cm^2 while across applied voltage 4V. This was on order less than Pt/BFO/PZT/Pt capacitor. The maximum saturation magnetization of capacitor (Pt/BFO/BNdT/Pt and Pt/BFO/PZT/Pt) was 2.47emu/cm^3. The BFO/BNdT/Pt had weakly saturation ferromagnetic and BFO/PZT/Pt had remanent magnetization.

Yan in 2011 [45] reported that in PZT modified BFO film a MBP region existed. In PZT (2% or 5%) modified BFO films appeared large domain size, less domain wall numbers and lower electrical conductivity (used in non-break down) than pure BFO film. This gave remanent polarization 76.8 (2%PZT) and 96.7μC/cm^2 (5% PZT). The modified BFO film showed modified phase structure and angle Bi—O, decreased the defect density and defect dipole complexes and different domain structure.

Uchida et al. in 2007 [46] prepared BFO thin film without using toxic Pb ferroelectric. They used rare earth ions ($La^{+3} and\ Nd^{+3}$) substituted in the place of Bi^{+3}. These substitutions reduces the ionic defect density (lattice), crystal ionic anisotropy and phase transition temperature. The leakage current density get reduced by rare earth metal replacement method. The remanent polarization of the P-E loop was 50 mC/cm^2.

Choudhary et al. in 2009 [47] synthesized nano-composite of BFO-PZT by solid state reaction (mechanical activation) method. They studied the frequency effect on the solid state electrolyte (BFO-PZT) with low frequency regions. The conductivity increases as corresponding frequency increased.

Chapter 3

EXPERIMENTAL DETAILS

3.1 Powder synthesis

The powder of BFO and PZT was synthesized by using sol gel method. The details of the preparation powder is given below.

3.1.1 Synthesize of BFO Process

In first step the Ferric Nitrate non-hydrate (0.2% mol), Bismuth Ferrite (0.2%) and 100 ml ethanol were mixed for one hour on magnetic strirrer. In second step dilute nitric acid was added dropwise. This sol was kept at room temperature for 24 hours. In this process, the Xero-gel powder was formed. The gel was kept at 300 ^{0}C to form powder.

3.1.2 Synthesize of PZT

Raw Materials: Lead nitrate (Pb{NO_3}$_2$), Zirconyl nitrate hydrate (Zr{NO_3}$_2$) and Titanium iso-propoxide Ti(OCH{CH_3}$_2$)$_4$ and ethanol were mixed for one hour on magnetic strirrer. Then dilute nitric acid was added dropwise. This sol was kept at room temperature for 24 hours. In this process, the Xero-gel powder is formed. The gel kept at 300 ^{0}C to form the powder.

3.1.3 Pelletization

The Stack of BFO and PZT was prepared by filling of the BFO and PZT powder respectively in the die of diameter 10 mm. The as filled powder was pressed under the pressure 10 ton using hydraulic press.

3.1.4 Sintering

The as pressed pellet was sintered in muffle furnace at 800 ^{o}C in ambient atmosphere for two hours. The heating and cooling rate were to fixed 5 ^{o}C/minute.

3.2 Charaterization Techniques:

3.2.1 Phase Identification

The phase identification of as prepared powder of BFO and PZT were carried out by XRD diffractometer. Phase analysis of the pure BFO and BFO-PZT composite carried out by X-ray diffraction (XRD) using CuKα radiation (λ = 1.54178 Å) (Philips X-pert PRO).

Brief description of XRD techniques is explained below:

The X-Ray is the one of the important and basic characterization technique which can be used in the solid state physics, material science and engineering. This technique is used to measure unit cell dimension and phase identification of the crystalline sample**.** It can be used in analyzing how an atom packs with other atoms in crystalline phase and can calculate the interatomic spacing and diffraction angles. Constructive Interference condition is shown in equation-

$$\textbf{\textit{Bragg's law: } n\,\lambda = 2d\,\sin\theta}$$

The *Bragg's diffraction law* was proposed by ***William Lawrence Bragg*** into the crystal structure analysis**.** ***Bragg*** and his father ***William Henry Bragg*** collimated to X-rays and it is diffracted from different crystallographic planes. This technique was based on the constructive interference of the electromagnetic and monochromatic X-Rays. When high energy photons are incident on an atom, the electrons absorb this energy and vibrate with the incident frequency of photons in the atomic regular positions. This Bragg's law is directly related to the X-ray wavelength, scattered angle (2θ) and the lattice spacing (d) of the crystalline materials. In crystal, atoms are arranged in a regular pattern. So, the few directions are possible in crystal, where the XRD shows constructive interference (Bragg's condition). The X-rays are electromagnetic radiation of wavelength ($1A^0$). If incident X-ray wavelengths match with the interatomic distance and satisfied with Bragg's law then this provides the figure print which is the characteristics of the crystalline sample. Fig. 3.1 explain the diffraction of X-rays from the lattice site atoms.

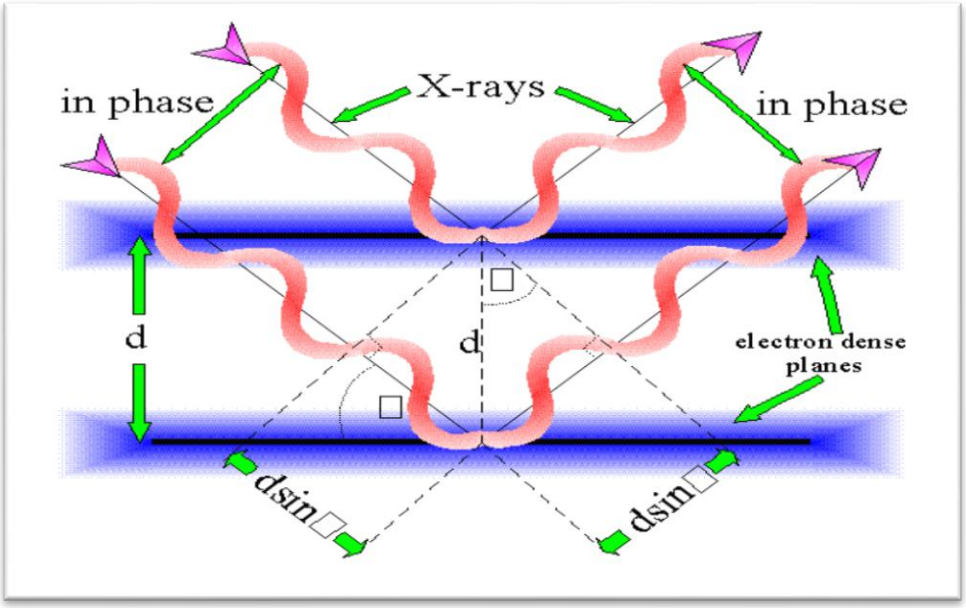

Fig. 3.1: Schematic of fundamental diffraction from lattice sites

The main parts of diffractor are X-ray tube, incident beam optics, goniometer, sample and sample holder, receiving side optics and detectors. The X-ray tube is the source of X-rays production. The incident beam optics is the part where the X-ray reaches before the interacting the sample. Goniometer contains the sample and moves the holder, optics and detectors. The receiving side optics is the part that contains the encountered X-rays. The detectors count the numbers of X-rays scattered by the sample. When the cathode ray tube is heated then electron beam is generated which get focused on copper target. These electron collisions of internal shell electrons gives the series of characteristic X-ray beam ($K_{\alpha 1}$, $K_{\alpha 2}$ and K_{β}). The both K_{α}'s have the same energies but K_{β} has a smaller energy than K_{α}. So, K_{β} is removed by a filter which situated on either side of the generator or detector side. The Cu-K_{α} radiation (1.5418Å) is mostly used in single crystal diffraction method. Fig. 3.2 shows the main parts of X-ray diffractometer given blow-

Fig. 3.2: X-ray diffractometer.

3.3 P-E loop Measurement

The measurement methods used have been developed over the years with advances in electronic hardware and software. The most often quoted method of hysteresis loop measurement is based on a paper by ***Sawyer and Tower***. A schematic of the experimental setup is shown in figure 3.5. Here the field applied across the sampleis attenuated by a resistive divider, and the current is integrated into charge by virtue of a large capacitor in series with the sample. Both these voltages are then fed into the X and Y axes of an oscilloscope to generate the P-E loop. The applied voltage was usually a sinusoid at mains frequency as this was the simplest method to generate the required voltage and current. The P-E loop of the pellet were measure by radiant model aixACCTTF-Analyzer 2000-

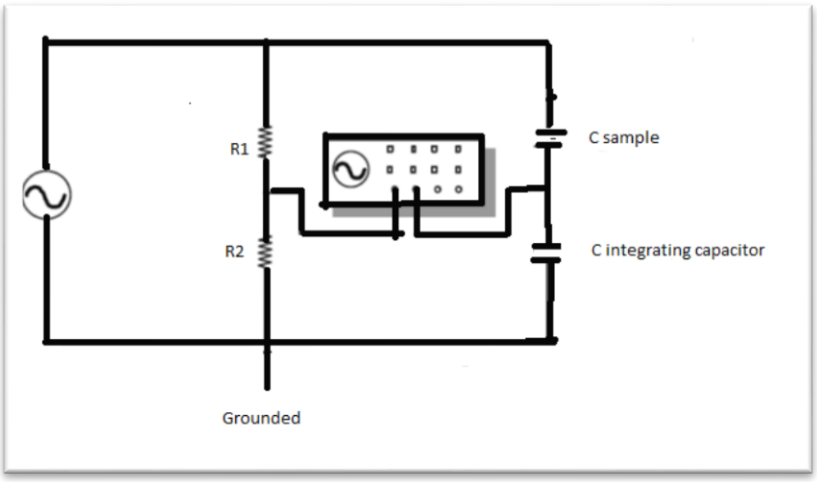

Fig. 3.3: P-E loop measurements (Schematic of *Sawyer Tower* circuit)[48]

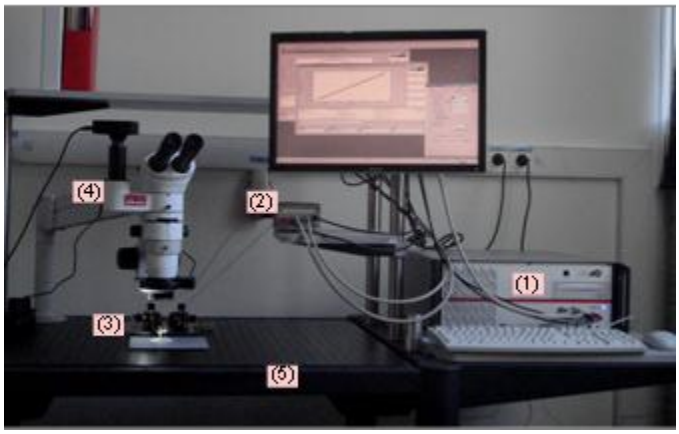

Fig.3.4: Dynamic and static P-E hysteresis loop measurment

Chapter 4

RESULTS AND DISCUSSION

4.1 X-ray Diffraction Pattern Analysis

Fig. 4.1 (a) and (b) shows the X-ray diffraction (XRD) pattern of BFO and PZT annealed at 800ºC respectively. Phase analysis of the pure BFO and PZT composite carried out by X-ray diffraction (XRD) using CuKα radiation (λ = 1.54178 Å) (Philips X-pert PRO). XRD results conform that BFO is polycrystaline in nature. All the peaks in the pattern of pure BFO corresponds to the distorted rhombohedral symetry perovskite-type with a space group (R3c) (JCPDS card No. 20-0169). However, the peaks in the pattern of PZT found corresponds to be tetragonal structure with (T, *P4 mm*) symetry. All the peaks in XRD pattern were indexed with (hkl) indices. There are no other impuriry phases, like $Bi_2Fe_4O_9/Bi_2O_3$. were found in the pure BFO. Also there is no other impurity phases were observed in PZT structure.

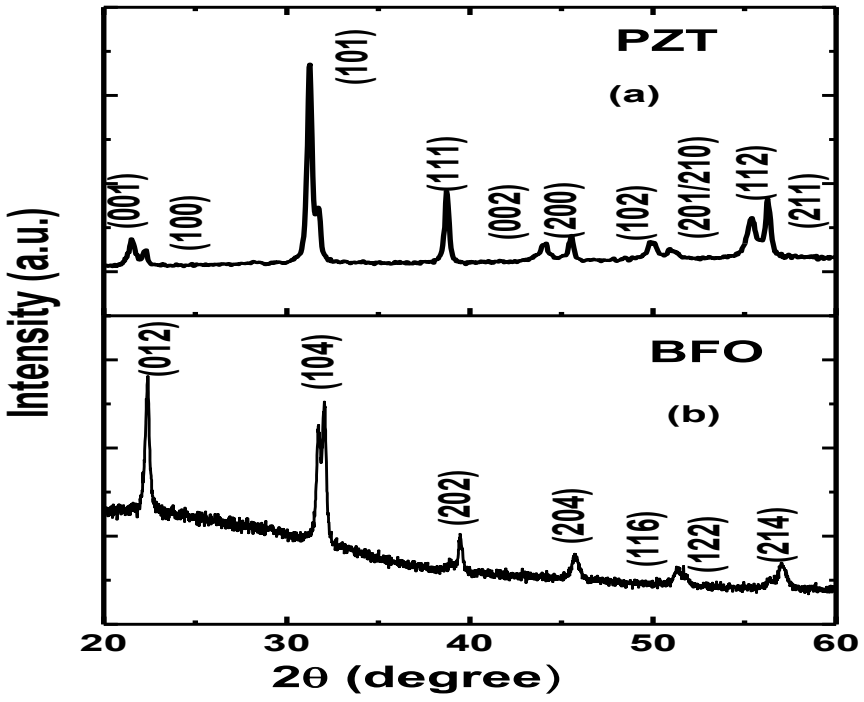

Fig. 4.1: the XRD patterns of pure PZT and BFO

4.2 Polarization-Electric Field Measurement of Pure BFO

Figure 4.2 shows the polarization vs. applied electric field (*P-E*) hysteresis loops of the pure BFO measured at room temperature at 1Hz. The BFO shows the desirable ferroelectric behavior. The remanent polarization (P_r) value measured for the pure BFO 12μC/cm^2.

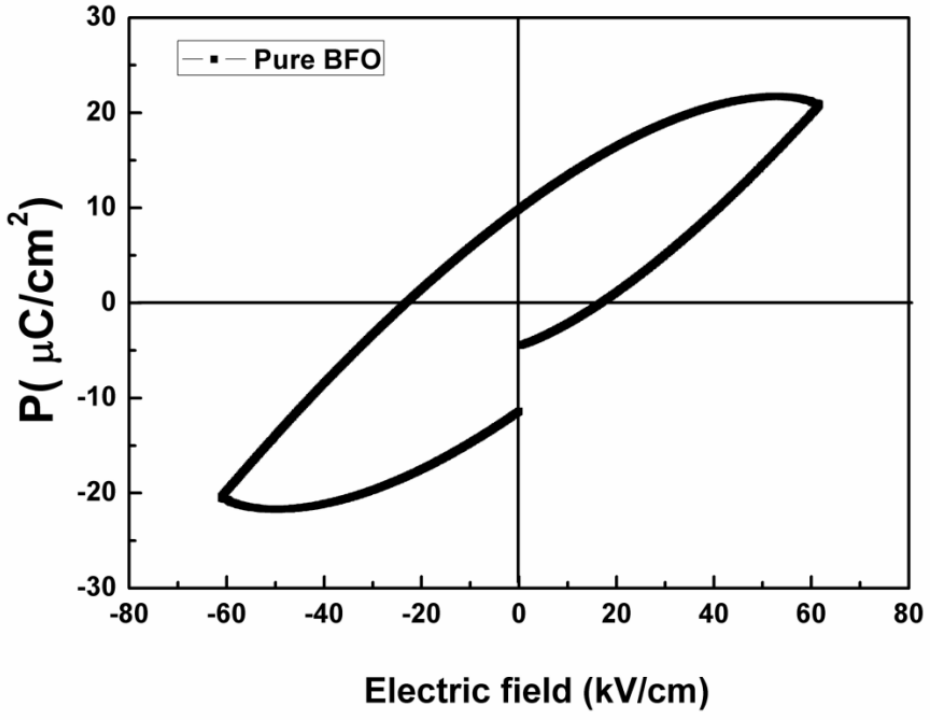

Fig. 4.2: Polarization-electric field hysteresis loops of pure BFO.

4.3 Polarization-Electric Field Measurement of Composite BFO-PZT Structure

Fig. 4.3 (a), (b), and (c) shows the ferroelectric polarization versus electric field (P-E) curves of the BFO-PZT composite measured at different frequency ranging from 1 kHz to 1Mz. The P-E loops of the composite shows well-defined hysteresis loop. The BFO-PZT composite exhibit improved ferroelectric behaviour than pure BFO. The remanent polarization (P_r) value measured for the pure BFO and BFO-PZT composite were found to be 12μC/cm^2 and 40μC/cm^2 respectivily. The PZT phase is responsible for the improve ferroelectric properties of the composite.

It is also seen that the there is a decrease in the value of remnant polarization (P_r) with the increase of applies field frequency. which is because of the jumping frequency of electric dipoles does not follow the alternating electric field beyond a certain critical frequency resulting the ferroelectric properties decreases**.**

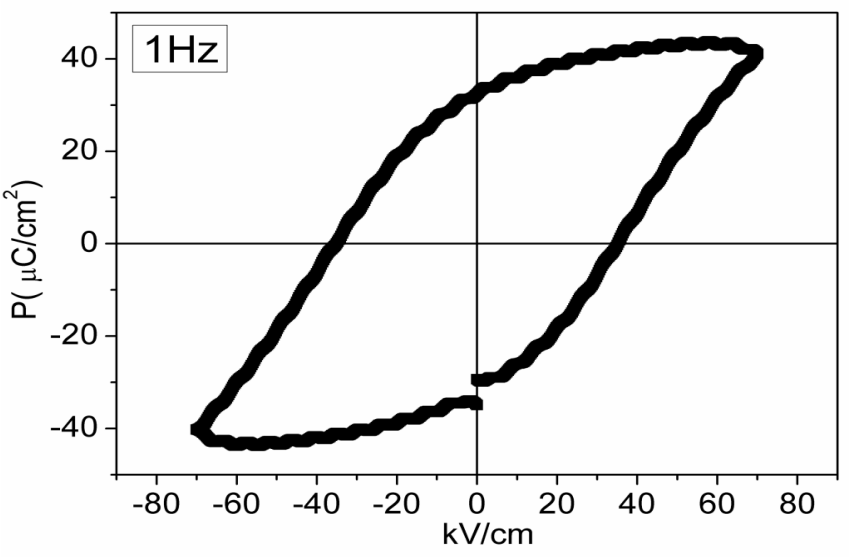

Fig. 4.3(a): Polarization-electric field hysteresis loops of BFO-PZT composite structure at 1Hz.

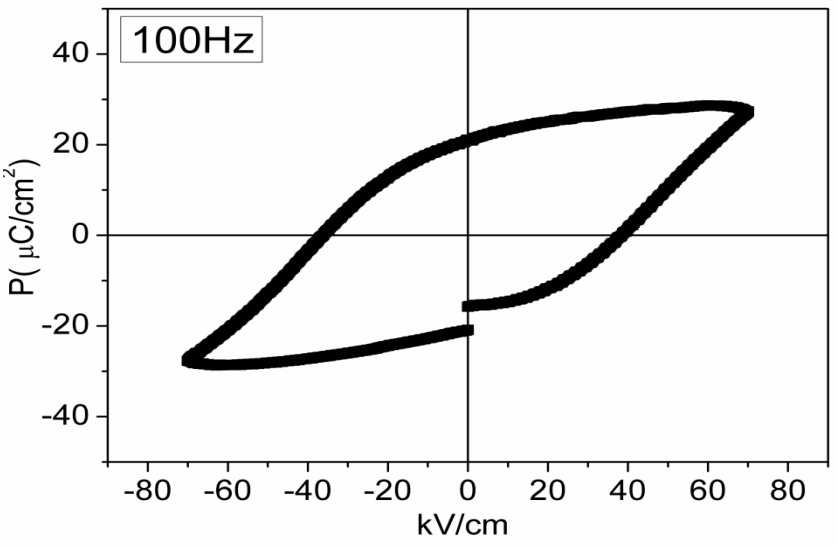

Fig. 4.3 (b): Polarization-electric field hysteresis loops of BFO-PZT composite structure at 100Hz.

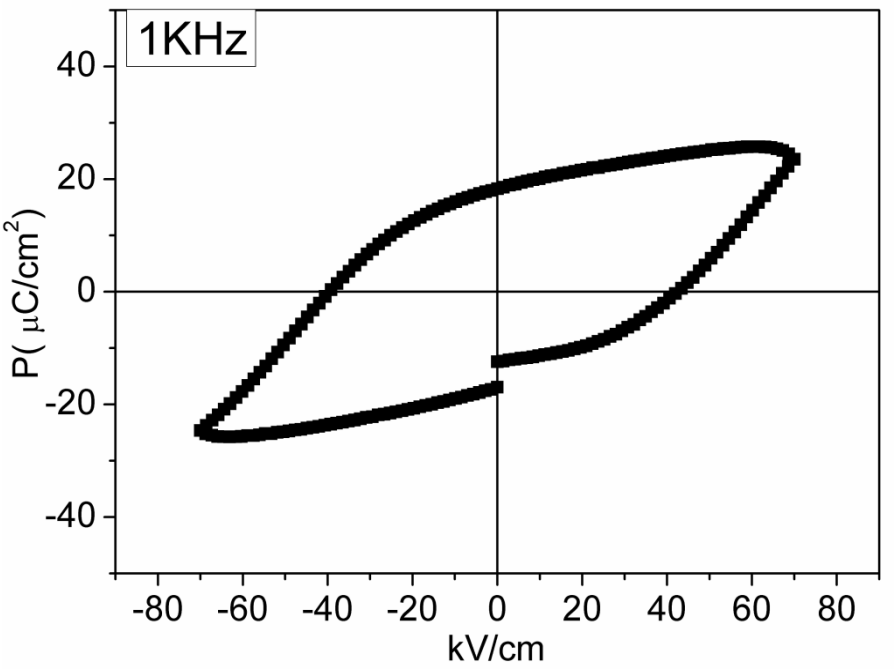

Fig.4.3(c): Polarization-electric field hysteresis loops of BFO-PZT composite structure at 1KHz.

4.4. Temperature dependent Dielectric Constant of BFO-PZT Composite

Fig.4.4 shows the temperature dependence of dielectric constant of BFO sintered at 800 ^{o}C. It can be seen that the dielectric constant increases with the increasing of temperature measured at different frequency and the temperature range of 300K $\leq T \leq$ 673 K. As the temperature increases, more charge carriers get excitation from their trapping centres and contribute to the polarization which in turn increases the dielectric constant of the composite. From the Fig.4.4, it is clear that the anomaly in dielectric constant found to be around critical temperaturete.

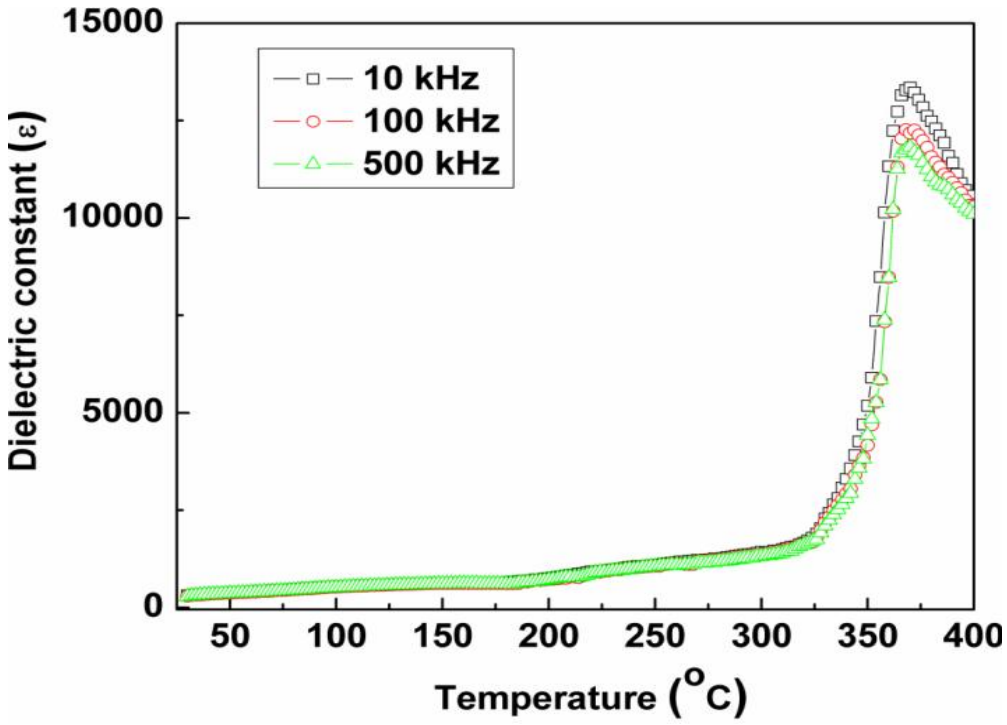

Fig. 4.4: Dielectric constant of BFO-PZTcomposite

4.5. Frequency dependent Dielectric Constant of Pure BFO and BFO-PZT Composite

Fig.4.5 shows the *R-T* frequency dependence dielectric constant of BFO and BFO-PZT composite in the frequency range of 100 Hz to 10 kHz. The dielectric value of constant is found to be higher for composite structure than pure BFO. It is also clear from Fig. 4.5 that increasing the frequency, the value of dielectric constant for pure BFO and BFO-PZT is found to be nearly constant. The values of dielectric constant for BFO and BFO-PZT composite sintered at 800^{o}C, were 240 and 290 respectively.

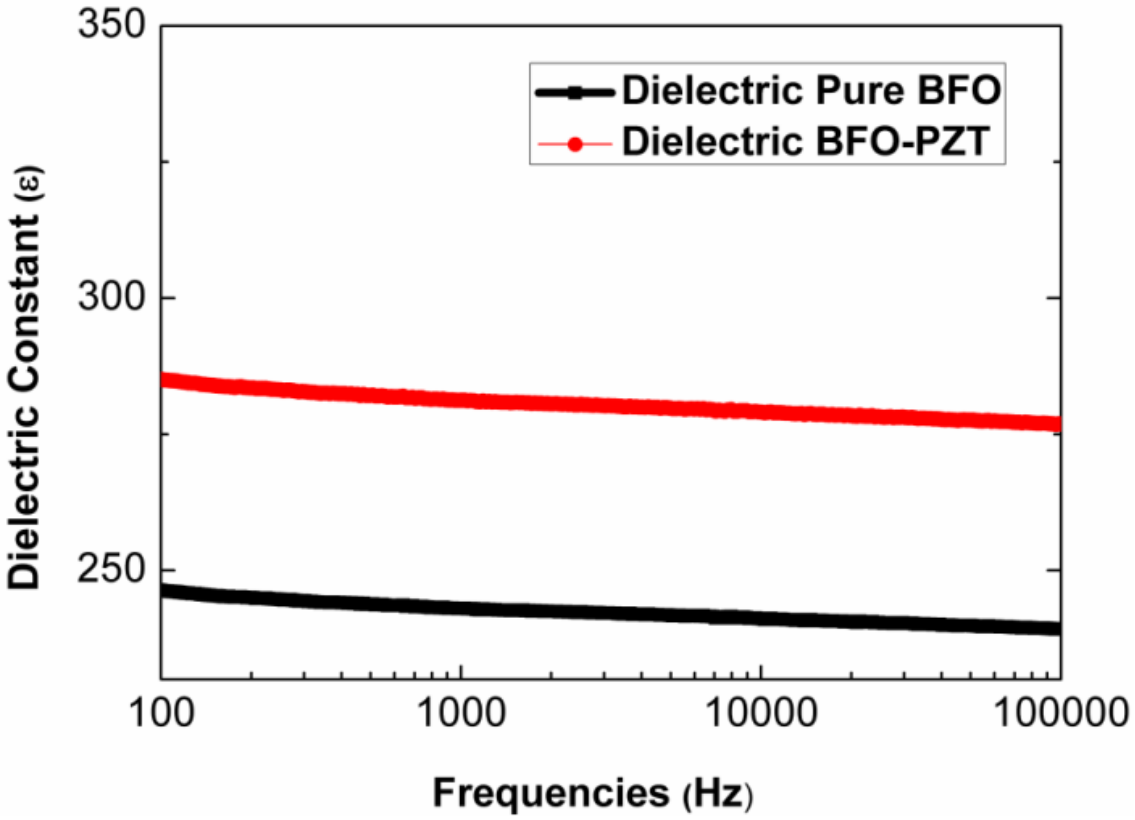

Fig.4.5: Dielectric constant pure BFO and BFO-PZT composite

Conclusion

Phase analysis of the pure BFO and PZT powders carried out by X-ray diffraction (XRD) Patterns. The results confirm pure phases of BFO and PZT powder without any impurity phase. The ferroelectric behavior of the BFO-PZT composite found to be increased with remnant polarization (40μC/cm^2) than pure BFO (12 μC/cm^2). The dielectric constant is higher in laminate composite as compared to pure BFO. The dielectric constant for BFO-PZT composite is 290 at room temperature. The dielectric constant found to be increased with increase in temperature range of 300K ≤ *T*≤ 673K at different frequencyIt is also seen that there is decrease in remnant polarization (*Pr*) with increase in applied electric field.

References

1. H. Schmid, Int. J. Magn., **4**, 337-362 (1973).

2. D. L. Fox and J. F. Scott, Phys. C, **10**, L329-331(1977).

3. J. F. Scott, Phys. Rev. B, **16**, 2329-2331(1977).
   s
4. G. A. Samara and J. F. Scott, Solid State Comm**., 21**, 167-170 (1977).

5. J. C. Maxwell, Phil. Trans. Res. Soc. Lond, **155**, 459-512 (1865).

6. L. D. Landau and E. M. Lifshitz, The Classical Theory of Field 2nd ed. (Pergomon London, 1962).

7. G. A. Smolenskii Sov. Et al., SSSR, Ser. Fiz, **25**, 1333 (1961).

8. P. Curie, J. physique, **3**, 393 (1894).

9. I. E. Dzyaloshinskii, Sov. Phys. JETP, **10**, 628 (1959).

10. R. Palia, Phys. Rev. B, **77**, 014110 (2008).

11. M. Valant et al., Chem. Mater., **19**, 5431(2007).

12. N. N. Krainik et al., Phys. Solid State, **8**, 654(1966).

13. H. Schmid private Communication.

14. D. Lebeugle, Ph.d. Thesis Saclay Inst. of Matter and Radiation (2007).

15. H. Bea et al., Appl. Phys. Lett., **87**, 072508 (2005).

16. J. Lou et al., Appl. Phys. Lett., **90**, 262908 (2007).

17. S. O. Leontsev and R.E. Eitel, J. Am. Ceram. Soc., **92**, 2957 (2009).

18. J. M. Moreau et al., J. Phys. Chem. Solids, **32**, 1315 (1971).

19. V. S. Filiper et al. Sov. Phys. Crystallogr., **5,** 913 (1960).

20. F. Kubel and H. Schmid , Acta Cryst**. B**, 46, 698 (1990).

21. J. D. Bucci et al. J. Appl. Crysl., **5,** 187 (1972).

22. Y. H. Chu et al., Mater. Today, **10**, 16-23 (2007).

23. Valasek, J. Phys. Rev., **17**, 422-3 (1922).

24. N. Tsubouchi et al., U.S. Patent no. 3699045 (1972).

25. H. Thurnauer, The Rochester Engineer, **21**, 74-5-77 (1942).

26. H. Thurnauer and Deaderick, J. U.S. Patent 2, **429**, 588 (1947, 1941).

27. Anthony R. West, "Solid State Chemistry and its Applications", Wiley and Sons (2005).

28. M. D. Durruthy-Rodriguez and J. M. Yanez-Limon, Elect. and Electro. Engg.- "Ferroelectris-Physical effect", book edit. Michael Lallart (2011).

29. B. Gerand et al. J. Solid State Chem., **29**, 429 (1979).

30. C. Williams and J. Ferrie, paper presented in 5th European Solid State Oxide Fuel Cell Forum, Lucerne, Switzerland (2002).

31. R. P. Choudhary et al., Appl. Phys. A, **86**, 131-138 (2000).

32. S. H. Jo et al., Nanoscale Res. Lett., 7 (2012).

33. Y. Wang et al., NPG Asia Mat., **2**, 61-68 (2010).

34. Y. W. Li, Appl. Phys. Lett., **87**, 182902 (2005).

35. S. Zhang et al., Appl. Phys., Express, **5**, 8041802 (2012).

36. S. P. Nam and S. G. Lee, Trans. Elect. Electro. Mat. (TEEM), **11**, 212-215 (2010).

37. S. H. Jo et al., Trans. on Elect. Elctro. Mat., **12**, 193-196 (2011).

38. D. Xie et al., Sci. in China Ser. E: Technological Sci., **52**, 10-14 (2009).

39. J. Lee and Lee, Mat. Res. Bull, **47**, 4 (2012).

40. C. Hyun and J. Lee, J. of KIEEME, **24**, 895-899 (2011).

41. Y. Wu and Yujie, Appl. Phys. Lett., **98**, 192915(3) (2008).

42. V. Stancu et al., Elsevier, **519**, 6269-6277 (2011).

43. S. H. Jo et al., J. of Ceram. Proc. Res., **13**, 38-41 (2012).

44. X. Wang, Adv. Mat. Res. Micro. And Nanotechno., **60-61**, 256-259 (2009).

45. F. Yan, J. of Appl. Phys., **110**, 114116-114116 (2011).

46. Uchida and Hiroshi, Appl. of Ferroelect., 138-141 (2007).

47. R. N. P. Choudhary et al., Mordern Phys. Lett. B, **33**, 2655 (2009).

48. C. B. Sawyer and C. H. Tower, Phys. Rev., **35**, 269 (1930)